Levels of P^{29} from $Si^{28}(p,p)Si^{28}$ and $Si^{28}(p,p')Si^{28*}$ †

J. VORONA,* J. W. OLNESS,‡ W. HAEBERLI,§ AND H. W. LEWIS
Duke University, Durham, North Carolina

(Received July 22, 1959)

Differential cross sections for the elastic and inelastic scattering of protons from Si^{28} have been measured at center-of-mass scattering angles of 167.7°, 141.3°, 90.0°, and 54.7° for proton energies between 1.4 and 3.8 Mev. Resonances were observed at proton energies of 1.66, 2.09, and 2.88 Mev, in addition to the resonances at 3.10, 3.34, 3.58, and 3.71 Mev which correspond to levels in P^{29} reported previously by other investigators from studies of the γ rays from $Si^{28}(p,p'\gamma)Si^{28}$. Differential cross sections and angular distributions for inelastic scattering to the 1.78-Mev first excited state of Si^{28} were also measured for proton energies above 3 Mev. Measurements were made with a gas scattering chamber containing silane (SiH_4) as the target gas. The elastic scattering data were analyzed in terms of the single-level approximation of the dispersion theory to determine the resonance parameters. This analysis, together with the analysis of the inelastic scattering cross sections and angular distributions, has resulted in the following assignments of resonance energies (Mev) and spins and parities for the resonance levels of P^{29}: 1.660 ($3/2^-$); 2.090 ($1/2^+$); 2.88 ($1/2^-$); 3.100 ($5/2^-$); 3.337 ($3/2^+$); 3.575 ($3/2^-$); and 3.711 ($3/2^+$). The large reduced elastic scattering widths of the p-wave resonances at 1.660 and 2.88 Mev suggest that these levels correspond to single-particle excitations of P^{29}.

I. INTRODUCTION

INFORMATION on the low-lying virtual levels of P^{29} has been obtained at Oak Ridge[1] from studies of the γ rays from the reaction $Si^{28}(p,p'\gamma_{1.78})Si^{28}$. Resonances for inelastic scattering, in the energy region below 4 Mev, were reported at laboratory proton energies of 3.10, 3.34, 3.58, and 3.71 Mev, with total widths of 12, 11, ~100, and ~80 kev, respectively. With enriched targets narrow resonances (total widths <4 kev) were observed at 2.64, 3.88, 3.93, and 3.97 Mev. Angular distributions of the 1.78-Mev γ rays with respect to the incident proton beam were measured for the four broad resonances. However, due to the ambiguities involved in the interpretation of the γ-ray angular distributions, the description of the level structure of P^{29}, in terms of spins and parities, and total and partial widths, was not complete.

The present investigation of the elastic and inelastic scattering of protons from Si^{28} was undertaken to provide a more complete description of P^{29}. The study extends over the range of incident proton energies from 1.4 to 3.8 Mev; the corresponding excitation energies in P^{29} lie between 3.8 and 6.4 Mev.

II. EXPERIMENTAL PROCEDURE

The proton beam from the Duke Van de Graaff accelerator was analyzed by a 90° electrostatic analyzer adjusted for a resolution of 0.1%. The beam entered a gas scattering chamber, described elsewhere,[2] through a thin aluminized Al_2O_5 foil. The chamber contained silane (SiH_4) at a pressure of about 3 mm Hg. Collimation of the beam was accomplished with two apertures 0.16 cm in diameter located 40 cm apart in the entrance tube and one aperture after the foil to eliminate protons scattered by the foil. The beam current was integrated in an evacuated collector cup isolated from the chamber by a 0.5 μ nickel foil.

The detector was a thin CsI crystal coupled to a Dumont 6292 photomultiplier tube. A precision slit system defined both the effective target volume and the acceptance solid angle of the detector. The number of elastically scattered protons was measured with an integral pulse-height discriminator set just below the elastic group. A ten-channel analyzer measured the inelastic protons and the flat background under this group was subtracted out.

The error introduced into the elastic cross sections by counting statistics and by uncertainties in the determination of the temperature and pressure of the gas and the geometry of the chamber was held to less than 3%.

The silane was generated[3] by adding Mg_2Si to dilute HCl in vacuum. The gaseous reaction products were passed through a series of filters to remove water and acid vapors and then fractionated to remove the higher silanes. The gas was stored in a glass cylinder and admitted to the scattering chamber through glass and copper tubing. Before admitting the silane, the chamber was pumped for several hours to remove the products of outgassing. Leakage rates were read with an oil-filled U-tube manometer. After the gas was admitted, the pressure showed a rise of about 3% per 10 hours. At the end of the 10-hour interval the chamber was refilled with fresh silane.

In order to calculate the number of silicon nuclei per

† This research was supported by the U. S. Atomic Energy Commission.

* Now with the U. S. Government.

‡ Now at the Aeronautical Research Laboratory, Wright Patterson Air Force Base, Ohio.

§ Now at the University of Wisconsin, Madison, Wisconsin.

[1] Cohn, Bair, Kington, and Willard, Phys. Rev. **99**, 644 (A) (1955); Willard, Bair, Cohn, and Kington, Bull. Am. Phys. Soc. Ser. II, **1**, 264 (1956).

[2] Olness, Haeberli, and Lewis, Phys. Rev. **112**, 1702 (1958).

[3] J. W. Mellor, *A Comprehensive Treatise on Inorganic and Theoretical Chemistry* (Longmans, Green, and Company, New York, 1947), Vol. 6.

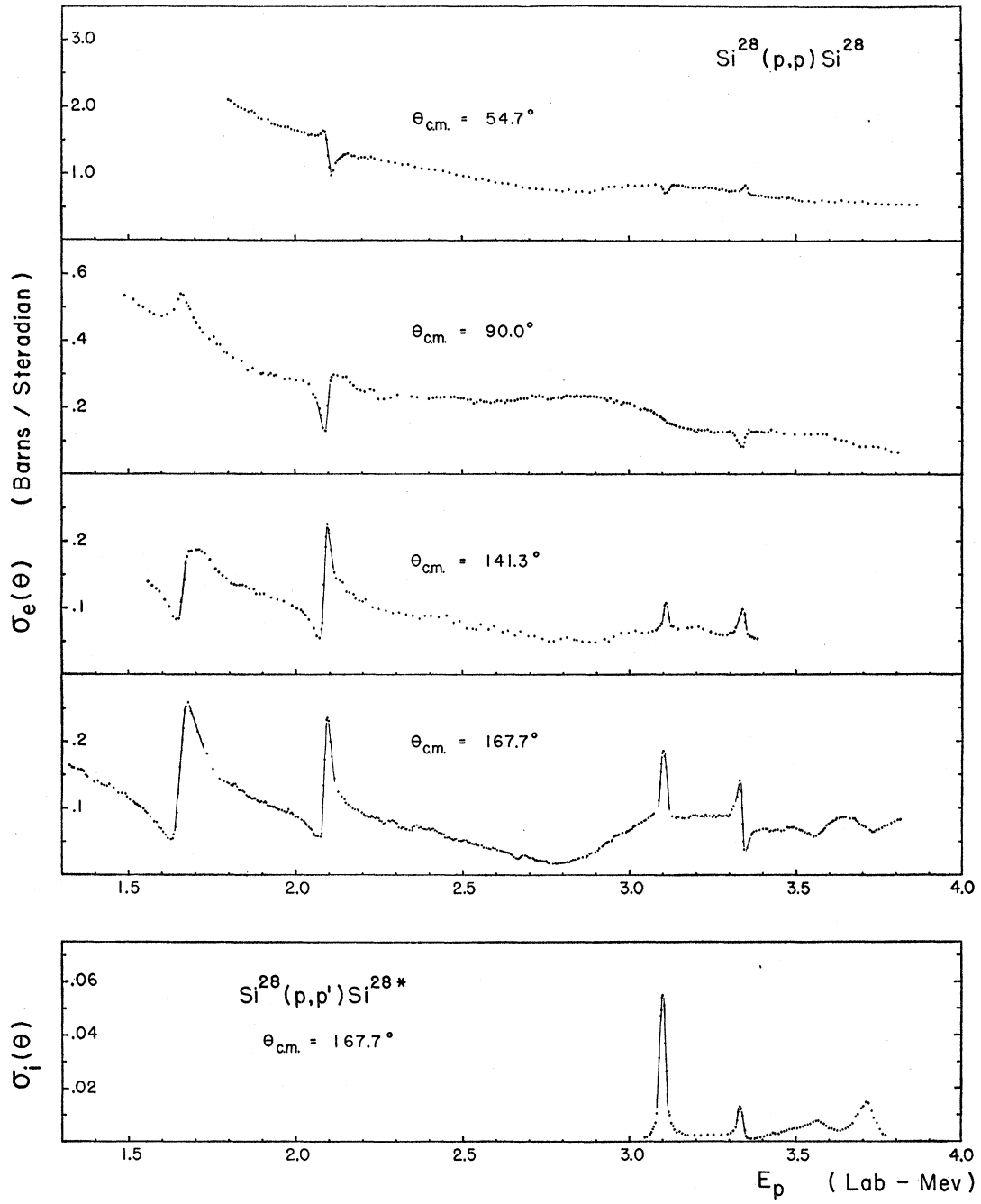

FIG. 1. Differential cross sections for $Si^{28}(p,p)Si^{28}$ and $Si^{28}(p,p')Si^{28*}$. The differential cross sections for elastic scattering are shown in the upper plot as a function of incident proton energy for the center-of-mass scattering angles of 167.7°, 141.3°, 90.0°, and 54.7°. The differential cross sections for inelastic scattering to the first excited state of Si^{28} are shown in the lower plot. Cross sections are given in the center-of-mass system, proton energies in the laboratory system of coordinates. The values plotted in the above figures are the nuclear cross sections as measured with a natural silicon target (92.2% Si^{28}). No corrections have been made for the presence of the isotopes Si^{29} and Si^{30}; however, it has been shown that the structure observed is due solely to resonance scattering from Si^{28}.

cm^3 in the target gas it was necessary to determine the amount of di-silane (Si_2H_6) present. This was done by placing the detector at an angle of 45° to the incident beam, measuring the separate counting rates due to elastic scattering from hydrogen and silicon, and using the known cross section[4] for $H^1(p,p)H^1$ to calculate the number of hydrogen atoms per molecule and hence the amount of di-silane. The results showed a 15% by

[4] H. R. Worthington, Ph.D. thesis, University of Wisconsin (unpublished).

volume admixture of Si_2H_6 in the SiH_4. From the amount of di-silane and from the relative vapor pressures of the various silanes it was estimated that the error introduced into the observed cross sections by neglecting to account for the presence of higher silanes, such as Si_3H_8, would be no more than 1%. The probable error in the differential elastic scattering cross sections, taking into account the uncertainties in the composition of the target gas, is about 6%. The probable error in the determination of the inelastic cross sections is about 12%.

The differential cross sections for elastic and inelastic scattering are shown in Fig. 1. The angles chosen are those for which the various Legendre polynomials vanish. The data for elastic scattering at 167.7° were obtained for energy increments of 4 kev or less in an initial search for resonance structure. The data for the other angles were obtained using larger steps. The energy scale has been corrected for energy losses in the entrance foil of the scattering chamber and in the target gas. For incident proton energies below 2.5 Mev the determination of absolute energies was made from a direct calibration in terms of the $Li^7(p,n)Be^7$ threshold at 1.881 Mev.[5] A lithium target was mounted on a rotating arm so that it could be placed at the center of the scattering chamber. Measurement of the neutron threshold, first with no gas in the chamber and then with a typical operating pressure, yielded a direct determination of the energy losses in the foil and target gas and of the absolute proton energy at the target volume. The values of the total energy loss at other bombarding energies were obtained by assuming an energy dependence given by the theory for stopping power.

Above 2.5 Mev the energy calibration was based on the position of the two narrow resonances at 3.100 and 3.337 Mev. These values for the resonance energies were determined with an uncertainty of ±3 kev from studies of the gamma rays from inelastic scattering in solid targets. The two calibration procedures agreed within 8 kev.

The energy spread of the incident proton beam at the effective target volume was estimated to be 5 kev for a bombarding energy of 2 Mev. A large part of this spread arises from straggling introduced by the energy losses in the foil and target gas. A specially prepared aluminum oxide foil[6] was chosen for this work in order to keep the energy loss in the foil as low as possible. The foils were coated with a thin evaporated layer of aluminum. They had an average lifetime of ten hours with a beam of 0.2 μa.

The angular distributions of the inelastically scattered protons are shown in Fig. 2. The measurements were made at bombarding energies corresponding to the resonance peaks in Fig. 1.

[5] Jones, Douglas, McEllistrem, and Richards, Phys. Rev. **94**, 947 (1954).
[6] K. Strohmaier, Z. Naturforsch. **6a**, 508 (1951).

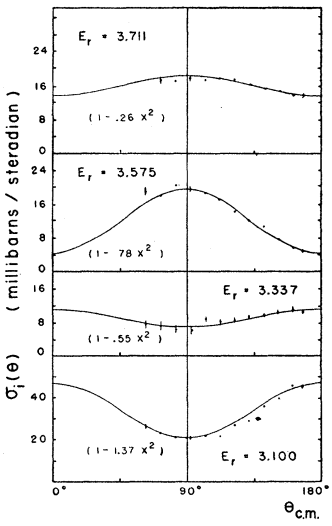

FIG. 2. Angular distributions of inelastic protons from $Si^{28}(p,p')Si^{28*}$. The measurements were made at the peaks of the inelastic scattering resonances shown in Fig. 1. The data have been fitted with distributions of the form $W_{pp'}(\theta)=1+A\cos^2\theta$; the coefficients of $\cos^2\theta=x^2$ are shown in the figure.

III. ANALYSIS OF EXPERIMENTAL DATA

The data for elastic scattering were analyzed in terms of the single-level approximation of the dispersion theory to determine the resonance energies, the total and partial widths, and the spins and parities of the resonance levels. The angular distributions of the inelastically scattered protons were analyzed in terms of the correlation theory to provide additional information on the angular momenta involved in the inelastic process. A summary of the results of these analyses is presented in Table I. For the lower lying resonances it was possible to obtain unique assignments of the level parameters from the elastic scattering data alone. For the higher lying resonances, these parameters could be obtained only from a full consideration of the data for both elastic and inelastic scattering.

The resonance energies and total widths of the resonances at 3.100, 3.337, 3.575, and 3.711 Mev have been reported by Willard *et al.*[1] from observations of the γ rays from inelastic scattering. The values of E_r and Γ given in Table I for these resonances were obtained from solid-target measurements made at Duke University. The values quoted are in good agreement with the results of Willard *et al.*

The angular distributions of the γ rays have also been measured at the four resonances in the inelastic cross section. No attempt is made here to present the complete analysis of all the γ-ray data. The following discussion is concerned primarily with the analysis of the proton distributions. However, in arriving at the conclusions expressed in the following sections, a knowledge of the general form of the γ-ray distributions was helpful. The measured γ-ray distribution for the level at 3.100 Mev exhibits a strong dependence on $P_4(\cos\theta)$. The angular distributions at the three higher lying

TABLE I. Resonance parameters for P^{29} from $Si^{28}(p,p)Si^{28}$ and $Si^{28}(p,p')Si^{28*}$. Columns 1 and 2 give the resonance energies E_r and the assignments of spin and parity j_λ^π for the levels of P^{29}. Column 3 gives the orbital angular momenta l_p of the incoming proton and the inelastically scattered proton $l_{p'}$. The total width Γ and partial elastic and inelastic scattering widths Γ_e and Γ_i are given in columns 4, 5, and 6. Columns 7 and 8 present the reduced widths for elastic and inelastic scattering as fractions of the Wigner single-particle limit $\gamma_w^2=3\hbar^2/2ma$. The last column lists excitation energies E_{ex} of P^{29}.

E_r (lab-Mev)	j_λ^π	$l_p; l_{p'}$	Γ (kev)	Γ_e (kev)	Γ_i (kev)	γ_e^2/γ_w^2	γ_i^2/γ_w^2	E_{ex} (c.m.-Mev)
1.660±0.010	3/2⁻	1	55±8	(∼55)		0.30		4.327
2.090±0.005	1/2⁺	0	18±4	(∼18)		0.015		4.742
2.880±0.080	1/2⁻	1	500±100	(∼500)		0.32		5.505
3.100±0.002[a]	5/2⁻	3; 1	12±1[a]	3.7±0.8	8.3±1.0	0.034	0.23	5.717
3.337±0.002[a]	3/2⁺	2; 0	11±1[a]	9.9±1.0	1.1±0.3	0.013	0.004	5.946
3.575±0.010[a]	3/2⁻	1; 1	90±15[a]	12.6±3.3	77 ±14	0.005	0.40	6.176
3.711±0.018[a]	3/2⁺	2; 0	70±12[a]	10.5±4.0	60 ±11	0.010	0.09	6.306

[a] These values of E_r and Γ were obtained from solid-target studies of the γ rays from inelastic scattering, as described in the text.

resonances involve only $P_2(\cos\theta)$; if there is a dependence of higher order it must be weak.[7]

The energy resolution of the present experiment was not high enough to determine the true shapes of the resonances at 3.100 and 3.337 Mev. The energy spread of the incident proton beam was of the order of 5 kev, while the total widths of these resonances are 12 kev and 11 kev, respectively. As a result, the measured resonance scattering amplitudes are somewhat less than would have been obtained with ideal resolution. The effects of this spread upon the measured cross sections do not seriously affect the following considerations which result in the assignments of total angular momenta and parity to the resonance levels. However, they were taken into account in arriving at the values of the partial widths for elastic and inelastic scattering.

III-A. ELASTIC SCATTERING: ANALYSIS

The general expression for the differential cross section for the elastic scattering of protons from a spin-zero target nucleus, for the case of a nonzero reaction width, has been discussed previously.[2] A brief outline is presented below. Under the treatment of the dispersion theory the cross section is specified in terms of a set of nuclear phase shifts δ_{lj} induced in the sub-partial waves having orbital angular momentum l and total angular momentum $j=l\pm\frac{1}{2}$. In the single-level approximation these nuclear phase shifts are represented as the sum of two contributions: a resonance phase shift β_{lj} and a potential scattering phase shift φ_l. The expression for δ_{lj} is

$$\delta_{lj}=\beta_{lj}+\varphi_l=\arctan\frac{\Gamma_\lambda/2}{E_\lambda+\Delta_\lambda-E}+\arctan\frac{F_l(\rho)}{G_l(\rho)}\bigg|_{\rho=ka}, \quad (1)$$

where k is the proton wave number, $\rho=kr$, where r is the separation of the target nucleus and the proton. $F_l(\rho)$ and $G_l(\rho)$ are the regular and irregular Coulomb wave functions (tabulated by Bloch *et al.*[8]), to be evaluated at the interaction radius $r=a$. The subscript λ is used to designate the particular level λ, having total width Γ_λ and characteristic energy E_λ. Δ_λ is the level shift.

In terms of these parameters, the cross section is most conveniently represented as a vector sum of the Rutherford scattering amplitude $\mathbf{R}$, which describes the purely Coulomb part of the scattering, and the various resonance scattering amplitudes $\mathbf{B}(l,j)$ as

$$\sigma(\theta)=\lambda\!\!\!^{-2}\left|\mathbf{R}+\sum_{l,j}\mathbf{B}(l,j)\right|^2+\lambda\!\!\!^{-2}\sin^2\theta\left|\sum_{l,j}\mathbf{B}'(l,j)\right|^2,$$

where

$$\mathbf{R}=-\tfrac{1}{2}\eta\csc^2(\theta/2)\exp[i\eta\ln\csc^2(\theta/2)],$$

$$\mathbf{B}(l,j=l\pm\tfrac{1}{2})=(j+\tfrac{1}{2})P_l(\cos\theta)\times\left[\sin\varphi_l e^{i\varphi_l}+\frac{\Gamma_{\lambda e}}{\Gamma_\lambda}\sin\beta_{lj}e^{i(\beta_{lj}+2\varphi_l)}\right]e^{i\alpha_l}$$

$$\mathbf{B}'(l,j=l\pm\tfrac{1}{2})=\mp\frac{dP_l(\cos\theta)}{d(\cos\theta)}\left[\frac{\Gamma_{\lambda e}}{\Gamma_\lambda}\sin\beta_{lj}e^{i(\beta_{lj}+2\varphi_l)}\right]e^{i\alpha_l},$$

and where

$$\eta=ZZ'/\hbar v;\quad \alpha_0=0,\quad \alpha_l=2\sum_t^l\arctan\frac{\eta}{t}\quad\text{for}\quad l\geqslant 1. \quad (2)$$

The indicated summations are to be carried out over all l and j. This expression shows that the strength of the resonance interference due to a level λ is proportional to the ratio of the partial width for elastic scattering $\Gamma_{\lambda e}$ to the total resonance width Γ_λ. The relationship between the total width Γ_λ, the partial widths $\Gamma_{\lambda s}$, and reduced partial width $\gamma_{\lambda s}^2$ is given by

$$\Gamma_\lambda=\textstyle\sum_s\Gamma_{\lambda s}=\sum_s(2k_s/A_{ls}^2)\gamma_{\lambda s}^2, \quad (3)$$

where $A_{ls}^2=F_l(\rho_s)^2+G_l(\rho_s)^2$. In the above expression the subscript s is used to designate the different channels available for dissociation of the compound nucleus.

A technique described previously was useful in the preliminary stages of the analysis. It has been shown

[7] H. B. Willard (private communication). Independent measurements performed at Duke University are in good agreement with these observations.

[8] Bloch, Hull, Brogles, Bouricius, Freeman, and Breit, Revs. Modern Phys. 23, 147 (1951).

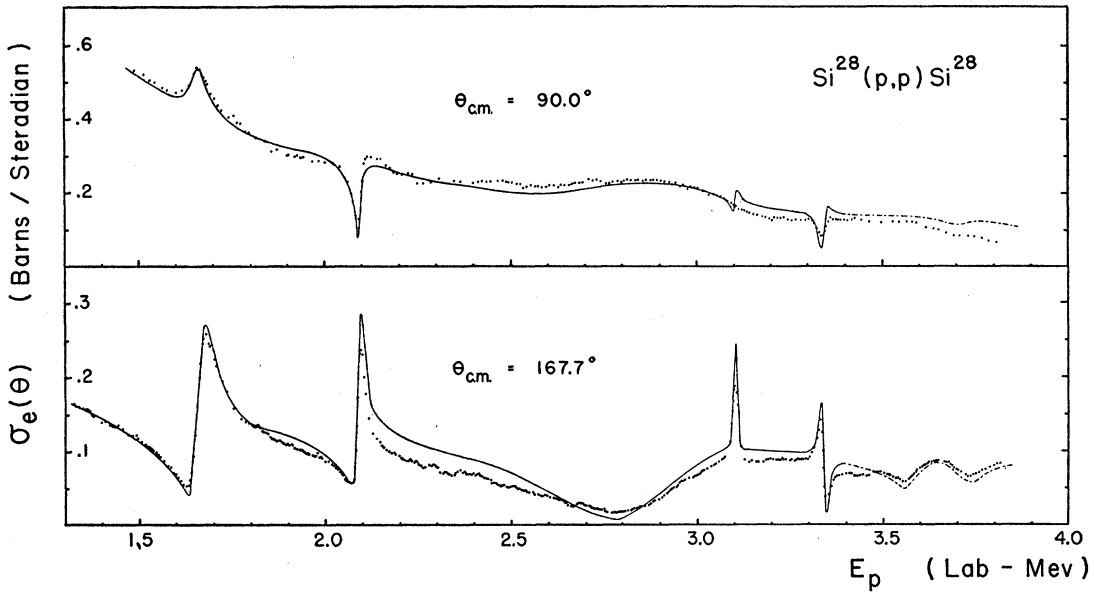

FIG. 3. Differential cross sections for $Si^{28}(p,p)Si^{28}$ at two angles. The solid curves show the cross sections calculated for the resonance parameters given in Table I. The dots give the experimental cross sections. The calculated cross sections have been adjusted (see text) to account for the presence in the target of the isotopes Si^{29} and Si^{30}.

that the dependence of the cross section upon a particular resonance phase shift β_{lj} may be written in the form

$$\sigma(\theta)=\lambda^2\{A(\theta)+B(\theta)\sin^2[\beta_{lj}+\xi(\theta)]\}, \quad (4)$$

where $\xi(\theta)$ is some constant phase shift (independent of energy), and A and B are related directly to the maximum and minimum cross sections at angle θ. Solutions for $(\beta_{lj}+\xi)$ may be obtained directly from the experimental data. The observed dependence may then be fitted with the single-level expression for β_l given by Eq. (1) to yield a set of best values for the resonance energy E_r, the total resonance width Γ_λ, and the constant phase shift $\xi(\theta)$.

The above technique was applied to the experimental data to obtain values for E_r and Γ_λ in first approximation. Equation (2) was then used to calculate the energy dependence of the cross section for the various possible assignments of l and j_λ. Comparison of the calculated interference patterns with those observed experimentally yielded tentative assignments of spins and parities for the resonance levels of P^{29}.

In the final stages of the analysis, Eqs. (1) and (3) were used to calculate the energy dependence of the cross section over the full energy interval studied in the experiment. The values of E_r and Γ_λ were then adjusted to yield the best fit to the measured cross sections. The assignments for the levels of P^{29}, namely, the assignments of resonance energies E_r, total widths Γ_λ, and total angular momenta and parities, are given in Table I. The cross sections calculated for these assignments are given by the solid curves of Fig. 3. Each resonance is discussed separately below.

The data shown in Figs. 1 and 3 give the cross sections measured for elastic scattering from natural silicon, which consists of 92.2% Si^{28}. The calculated curves presented in Fig. 3 have been adjusted to account for the presence of Si^{29} and Si^{30} by assuming that their contributions to the measured cross sections arise from pure Coulomb scattering. The net effect of this adjustment is that the resonance amplitudes observed in Fig. 3 represent only 92% of the resonance amplitudes to be expected for pure Si^{28}.

1.660 Mev

The preliminary phase-shift analysis based on Eq. (4) yields the values $E_r=1.660\pm0.005$ Mev, $\Gamma=55\pm6$ kev. The largest uncertainty in the determination of the absolute resonance energy arises from the uncertainty in the determination of the energy scale of Fig. 1, which involves rather large corrections for energy losses in the Al_2O_5 foil and in the target gas. The symmetric peak observed at 90° suggests that the resonance involves p-wave formation; the observed interference patterns at the remaining angles of observation bear out this assumption. Accordingly, cross-section calculations were carried out to determine the interference patterns expected for assignments of $1/2^-$ and $3/2^-$. Either assignment will fit the data for 90°, but the data for 167.7° and 141.3° can be fitted only with the $3/2^-$ assignment. The calculated curves for the $3/2^-$

assignment, shown for two angles in Fig. 3, are in good agreement with the measured cross sections at all angles.‖

2.090 Mev

The strong interference dip observed at 90° suggests that the resonance involves $l=0$ or $l=2$ formation of an even-parity resonance. The observed peak at 167.7° can be used to rule out the possibility for the $l=2$ assignment, which must necessarily exhibit a strong interference dip at this angle. One is thus left with a $1/2^+$ assignment, which fits the experimental data quite well at all angles. The phase-shift analysis gives the resonance energy and total width as 2.090±0.003 Mev and 18±4 kev, respectively.

2.88 Mev

The effects of this level are most clearly seen in the cross section for 167.7°, which exhibits a broad dip and subsequent rise in the region of the resonance energy, and from the 90° cross section, which exhibits a broad peak in the region of 2.9 Mev. The analysis based on Eq. (4) yields the following estimates for the resonance parameters: $E_r \cong 2.90 \pm 0.06$ Mev, $\Gamma \cong 450 \pm 150$ kev. The broad peak observed at 90° rules out the possibilities for s-wave or d-wave formation, and strongly suggests p-wave formation of a $3/2^-$ or $1/2^-$ level. The possibility for f-wave formation can be ruled out from the Wigner criterion for reduced widths. From the observed scattering amplitudes at 167.7° the resonance is clearly due to $l=1$ formation of a $1/2^-$ level of P^{29}. The cross sections calculated for these assignments are in good agreement with the experimental cross sections, as shown in Fig. 3. The effects of this particular level on the differential cross sections for 141.3° are not readily apparent from the experimental data, since the coherent term of Eq. (3) exhibits an interference dip, whereas the incoherent term exhibits a peak of almost equal amplitude. The resultant cross section shows almost no evidence of the effects of the 2.88-Mev resonance. However, the effects *are* important at 54.3°, where there is a broad energy dependence similar to but weaker than that observed in the data for 167.7°.

3.100 Mev

It has been pointed out earlier that the values for the resonance energy and total width given in Table I were obtained from separate studies of the γ rays. The analysis of the elastic scattering data, using only the energy calibration obtained from the $Li^7(p,n)Be^7$ threshold measurement described above, yields the values $E_r = 3.100 \pm 0.008$ Mev, $\Gamma = 14 \pm 3$ kev, in reasonably good agreement with the values given in Table I.

‖ *Note added in proof.*—Polarization measurements have been made on elastically scattered protons from Si^{28} which support the assignments $\frac{3}{2}^-$ and $\frac{1}{2}^+$ for the resonances at 1.660 and 2.090 Mev, respectively. Sorokin, Val'ter, Malakhov, and Taranov, Soviet Phys. (JETP translation) **8**, 969 (1959).

The symmetric appearance at 167.7° suggests that the resonance is due to f-wave formation of a $5/2^-$ or $7/2^-$ level. The possibilities for all other assignments can be excluded. The data for 54.9° are quite useful for this purpose. At this angle the Rutherford term of Eq. (3) is by far the largest contributor to the cross section, and the resonance interference pattern is determined primarily by the interference between the Rutherford term and the particular resonance term; the effects of neighboring levels are quite small. The observed dip at this angle is consistent only with p-wave or f-wave formation, since a d-wave resonance is expected to exhibit a symmetric peak, whereas an s-wave resonance is expected to exhibit an asymmetry similar to that observed for the $1/2^+$ resonance at 2.090 Mev. The possibility for p-wave formation may be ruled out on the basis of the symmetric peak observed at 167.7°, since a p-wave resonance necessarily gives rise to severe destructive interference at this angle.

One is left with possible assignments of $5/2^-$ and $7/2^-$. The measured scattering amplitude at 167.7°, which is proportional to $(j+1/2)P_l(\cos\theta)\Gamma_e/\Gamma$, leads to a value Γ_e/Γ of the order of 0.2. However, this value is only approximate, since the observed maximum and minimum of the resonance are influenced by the limited experimental resolution, as was pointed out above. From a full consideration of the remaining angles of scattering, the $5/2^-$ assignment is preferred; however, the $7/2^-$ assignment cannot be completely excluded on the basis of the elastic scattering data alone. The curves presented in Fig. 3 were calculated for a $5/2^-$ assignment, assuming the ratio $\Gamma_e/\Gamma = 0.31$ obtained from the analysis of the inelastic scattering data presented in Sec. III-B. This assignment is seen to fit reasonably well at 167.7°. The disagreement observed at 90° suggests that the p-wave phase shifts at this energy are not correct. The calculated curve can be made to agree reasonably well with the experimental data by adjustment of the $1/2^-$ phase shift within limits corresponding to the uncertainties given for the resonance energy and total width of the 2.88-Mev resonance energy. With the phase shifts used, the $7/2^-$ assignment gives appreciably larger disagreement at 90° than that obtained with the $5/2^-$ assignment.

3.337 Mev

The analysis of this resonance proceeds in a manner similar to that presented for the resonance at 3.100 Mev. The observed dip at 90° suggests s-wave or d-wave formation; the possibility for s-wave formation can be ruled out on the basis of the measured asymmetry for 167.7° which agrees quite well with that calculated for a d-wave assignment, whereas that calculated for an s-wave assignment exhibits an asymmetry in the opposite sense. The curves presented in Fig. 3 were calculated for the d-wave $3/2^+$ assignment with the parameters given in Table I. Again, it is not possible to rule out completely the $5/2^+$ assignment on the basis

of the elastic scattering data alone; however, the $3/2^+$ assignment is preferred.

3.575- and 3.711-Mev Resonances

From the data for elastic and inelastic scattering presented in Fig. 1, and from Eq. (3), it is evident that for these two resonances the partial elastic scattering widths represent only small fractions of the total widths. Since the resonances appear only weakly in the elastic scattering cross sections, and also because of the large overlap between the two levels, the analysis of the elastic scattering data alone is not able to provide unambiguous assignments for these levels.

For the resonance at 3.575 Mev, the initial dip and subsequent rise at 167.7° suggest that the resonance involves p-wave formation of a $1/2^-$ or $3/2^-$ level. For the resonance at 3.711 Mev, the fact that the dip occurs *after* the resonance energy, suggests d-wave formation of a $3/2^+$ or $5/2^+$ level. From the observed maximum and minimum cross sections it is calculated that, for both resonances, the ratio Γ_e/Γ is of the order of 0.15.

The assignments given in Table I are the results of the complete analysis of both elastic and inelastic scattering. The dotted curves of Fig. 3 show the cross sections calculated for these assignments. The accuracy of these calculations is considerably less than the accuracy obtained in the calculation of the solid portions tilus of the curves. However, the results indicate that the curves calculated with the assignments in Table I are consistent with the experimental data. The magnitudes and shapes of the interference patterns are seen to agree semiquantitatively with those observed in the experimental cross sections.

III-B. INELASTIC SCATTERING: ANALYSIS

The inelastic scattering cross sections are shown in Figs. 1 and 2. The angular distributions of the inelastically scattered protons have been fitted with distribution functions of the form $W_{pp'}(\theta)=1+A\cos^2\theta$, which are shown by the solid curves of Fig. 2. The coefficients of $\cos^2\theta$ required to fit the data are also given.

A complete discussion of the methods of analysis has been presented in a previous paper,[2] and will not be covered in detail here. The relationship between the measured inelastic scattering cross sections and the resonance energies and total and partial widths may be obtained (for the case of an isolated resonance) from the general expression for the total inelastic scattering cross section

$$\sigma_i=\pi\lambda^2\frac{2j_\lambda+1}{(2s+1)(2I+1)}\frac{\Gamma_e\Gamma_i}{(E_r-E)^2+(\Gamma/2)^2}. \quad (5)$$

The values for σ_i were obtained from the data presented in Fig. 2 using

$$\sigma_i=\int\sigma_i(\theta)d\Omega,$$

and assuming the angular dependence given by the solid curves.

The relationship between the differential cross sections and the angular momenta involved in the inelastic scattering process is obtained from the correlation theory. For an isolated resonance, the correlation is completely specified in terms of the set of quantum numbers l, j_λ, l', s' and the known spins and parities of the target nucleus $Si^{28}(0^+)$ and the residual excited nucleus $Si^{28*}(2^+)$. In the following we consider the individual resonances in the light of the information made available by the foregoing analysis of the elastic scattering. Since the latter has placed definite restrictions on the possible assignments, we need only choose between the remaining ones.

3.100 Mev

The analysis of the elastic scattering shows that the resonance is due to f-wave formation of a $5/2^-$ or $7/2^-$ level. The measured angular distributions of the inelastically scattered protons can be fitted exactly with the assignment $j_\lambda{}^\pi=5/2^-$, $l'=1$, assuming a mixing ratio for the channel spins 3/2 and 5/2 of 0.90 to 0.10. The experimental data cannot be fitted with the $7/2^-$ assignment.

3.337 Mev

The analysis of the elastic scattering has limited the level assignment to either $3/2^+$ or $5/2^+$, with $3/2^+$ preferred. In this case, the angular distribution of the inelastically scattered protons provides no new information, since $l'=0$ for both cases and the angular distributions are expected to be isotropic. The observed anisotropy in the measured distribution presented in Fig. 2 can be explained as arising primarily from interference between the resonance scattering and the off-resonance scattering. Evidence for such interference is also observed in the excitation curves of Fig. 1: the cross section is *not* symmetric about the resonance energy, but exhibits a tail on the low-energy side and a definite dip on the high-energy side. This would suggest a coherent interference between resonance and off-resonance scattering. If the off-resonance scattering is due primarily to the odd-parity levels at 3.100 and 3.575 Mev, this would predict that the angular distribution of the inelastically scattered protons at 3.337 Mev should exhibit a dependence on $\cos\theta$. However, the data do not extend to small enough angles to determine the coefficient of this term, and they have been fitted instead with the simple distribution given previously.

The above arguments are presented only to show that the measured distribution is indeed consistent with the suggested assignment of $3/2^+$ or $5/2^+$, $l'=0$. In this case, the γ-ray distributions are completely specified by the statement of the total angular momentum of the resonance level. The distribution calculated for the

$3/2^+$ assignment exhibits a simple dependence involving only $\cos^2\theta$, in good agreement with the experimental data, while the distribution calculated for the $5/2^+$ assignment exhibits a strong dependence on $\cos^4\theta$, in disagreement with the measured distribution. On the basis of this information, the level is assigned total angular momentum and parity $3/2^+$.

3.575 Mev

The elastic scattering analysis has suggested that the resonance is due to p-wave formation of a $1/2^-$ or $3/2^-$ level. The measured proton distribution can be fitted exactly assuming $j^\pi=3/2^-$, with a channel-spin mixing ratio 3/2 to 5/2 of 0.90 to 0.10. The observed anisotropy rules out conclusively the possibility for an assignment $1/2^-$. The possibilities $3/2^+$ or $5/2^+$ are excluded also since these necessarily involve $l'=0$, giving isotropic distributions. An admixture of enough contribution from $l'=2$ to reproduce the observed anisotropy in the calculated distributions would yield a reduced inelastic scattering width exceeding the single-particle limit. Assignments of $5/2^-$ and $7/2^-$ can be excluded from a re-examination of the elastic scattering data. The observed peak height in the inelastic scattering cross section requires, for either of these assignments, that the elastic scattering width be considerably less than the inelastic scattering width. It is not possible, with such a small value of the elastic scattering width, to reproduce the marked interference observed in the elastic scattering cross section at 167.7°. The cross sections and distributions calculated for the $3/2^-$ assignment match the measured curves quite well.

3.711 Mev

The data for elastic scattering have suggested that the resonance most probably involves d-wave formation of a $3/2^+$ or $5/2^+$ level. The magnitude of the observed anisotropy in the inelastic scattering proton distribution can be accounted for almost wholly as due to an incoherent contribution from the lower lying $3/2^-$ level at 3.575 Mev, in which case the inelastic scattering from the 3.711-Mev level is isotropic. In this case, then, it is not possible to decide between the $3/2^+$ and $5/2^+$ assignments, since both involve $l'=0$ and result in isotropic distributions. However, the calculated γ-ray distribution for the $3/2^+$ assignment shows a simple dependence of the form $1+\cos^2\theta$, in agreement with the reported distribution, whereas that calculated for a $5/2^+$ assignment exhibits a strong dependence on $\cos^4\theta$, in strong disagreement with the measured distribution. Although the assignments $1/2^-$ or $1/2^+$ also result in isotropic proton distributions, the measured peak height in the inelastic scattering cross section is larger than can be obtained for a $j_\lambda=1/2$ assignment. The maximum inelastic scattering resonance amplitude is obtained for $\Gamma_e=\Gamma_i=\Gamma/2$. However, such a large elastic scattering width predicts much stronger interference effects in the elastic scattering cross section than are observed. The possibilities for assignments involving $j_\lambda \gtrsim 5/2$ can be tentatively excluded on the basis of the observed isotropy of the inelastically scattered proton distribution. Upon correlating the results of the proton and γ-ray angular distribution measurements, no doubt remains as to the correctness of the $3/2^+$ assignment.

TABLE II. Results of analysis to determine partial widths for elastic and inelastic scattering. The solutions for Γ_i/Γ in column four are the best values obtained from an analysis of the inelastic scattering data. The solutions given in column five for $\Gamma_i/\Gamma=1-\Gamma_e/\Gamma$ were obtained from an analysis of the elastic scattering data.

E_r (Mev)	Γ (kev)	j_λ^π	Γ_i/Γ	$\Gamma_i/\Gamma=1-\Gamma_e/\Gamma$
3.100	12	$5/2^-$	0.69 ± 0.06[a]	(0.78)
3.337	11	$3/2^+$	0.10 ± 0.02[a]	(0.55)
3.575	90	$3/2^-$	0.86 ± 0.03[b]	0.85 ± 0.08
3.711	70	$3/2^+$	0.85 ± 0.04[b]	0.85 ± 0.08

[a] Determined by area analysis.
[b] Determined by peak height analysis.

As a final consideration, the excitation curves and angular distributions were analyzed to yield values for the partial elastic and inelastic scattering widths. The results, shown in Table II, were obtained by two different methods: (1) from an analysis based on the observed peak heights in the inelastic scattering cross section, and (2) from an area analysis of the inelastic scattering data of Fig. 1. Upon taking into account the effects of the experimental resolution, the results of (1) have been shown to be in reasonable agreement with the results of (2). The analysis of the inelastic scattering data alone allows two solutions for Γ_i and Γ_e, since the inelastic scattering cross section is proportional to the product $\Gamma_i\Gamma_e$. Only the proper set of solutions for Γ_i/Γ are given in Table II. (The alternative solutions consist of the set of values given by $1-\Gamma_i/\Gamma$.) Also included in Table II are the results of the calculations for the ratio $\Gamma_i/\Gamma=1-\Gamma_e/\Gamma$ obtained from the analysis of the elastic scattering data, based on Eq. (2). Although these values are of somewhat lower accuracy, due to the effects of the limited energy resolution and to the uncertainties involved in the determination of the interference effects, they indicate quite clearly the proper set of solutions for Γ_i and Γ_e.

RESULTS AND CONCLUSIONS

The results of the present analysis of $Si^{28}(p,p)Si^{28}$ and $Si^{28}(p,p'\gamma)Si^{28}$, including the assignments for the levels of the compound nucleus P^{29}, are presented in Table I. The values given for the total and partial widths are the values calculated at the resonance energies given. The reduced widths for elastic and inelastic scattering are given as fractions of the Wigner single-particle limit $\gamma_w^2=3\hbar^2/2ma$. The interaction radius used in these calculations was that given by $a=1.45(A^{1/3}+1)\times10^{-13}=5.85\times10^{-13}$ cm. The excita-

tion energies in the compound nucleus P^{29} are also given in Table I. The present experiment has covered the range of excitation energies from 3.8 to 6.4 Mev.

From the large reduced *elastic* scattering widths for the $3/2^-$ level at 4.33 Mev and the $1/2^-$ level at 5.51 Mev, it is suggested that these levels arise primarily as single-particle excitations of a ground-state Si^{28} core plus a proton. In particular, in view of the excitation energies and splittings, it is suggested that these levels correspond to the $2P_{3/2}$ and $2P_{1/2}$ excitations, respectively.

Conversely, the large reduced *inelastic* scattering widths observed for the levels at 5.717 and 6.176 Mev would seem to suggest that these levels arise primarily as single-particle excitations of an excited Si^{28} core plus a proton.

PHYSICAL REVIEW VOLUME 116, NUMBER 6 DECEMBER 15, 1959

Differential Elastic Scattering of 14-Mev Neutrons by Zn, Sn, Sb, Pb, and Bi†

L. A. RAYBURN*
Argonne National Laboratory, Lemont, Illinois
(Received July 20, 1959)

Differential elastic scattering cross sections in the angular interval from 10° to 165° have been measured for Zn, Sn, Sb, Pb, and Bi. The experimental measurements are corrected for multiple scattering and the finite angular resolution by Monte Carlo methods. The corrected cross sections are compared with theoretical values computed by use of a complex potential with a spin-orbit term.

INTRODUCTION

DURING the past few years considerable effort has been expended in measuring differential elastic scattering cross sections at various energies for both neutrons and protons. These measurements have stimulated the development of various complex potential nuclear models[1–6]; and the partial successes obtained with these models have in turn been instrumental in causing more extensive and accurate measurements to be made. Much work has been done with 14-Mev neutrons[7–19] because the $H^3(d,n)He^4$ reaction is a convenient source of neutrons and also because the experimentally measured differential cross sections can be directly compared with theoretical predictions. (The elastic scattering cross section consists of a shape elastic part and a compound elastic part,[2] these being experimentally indistinguishable. However, for 14-Mev neutrons the compound elastic part is expected to be so small that the elastic scattering is essentially all shape elastic.)

The earlier measurements were confined mainly to scattering in the forward direction because of the formidable experimental difficulties encountered in measuring the cross sections at large angles. Many of these difficulties have been circumvented in various ways within the past two years so that reasonably accurate differential cross-section measurements have now become available over most of the angular range for a large number of elements. The measurements in the present paper cover the angular range from 10° to 165° for five elements. Preliminary reports of some of these measurements have been given previously.[15]

EXPERIMENTAL DETAILS

By using the associated-particle technique in conjunction with millimicrosecond electronic circuitry, we reduced the background problems inherent in this type of work to such an extent that cross-section measurements could be made within reasonable counting times. The experimental arrangement is shown in Fig. 1.

† Work performed under the auspices of the U. S. Atomic Energy Commission.
* Now at the University of Georgia, Athens, Georgia.
[1] R. D. Woods and D. S. Saxon, Phys. Rev. **95**, 577 (1954).
[2] Feshbach, Porter, and Weisskopf, Phys. Rev. **96**, 448 (1954).
[3] Culler, Fernbach, and Sherman, Phys. Rev. **101**, 1047 (1956).
[4] Bjorklund, Fernbach, and Sherman, Phys. Rev. **101**, 1832 (1956).
[5] F. Bjorklund and S. Fernbach, Phys. Rev. **109**, 1295 (1958).
[6] Luk'ianov, Orlov, and Turovtsev, J. Exptl. Theoret Phys. U.S.S.R. **35**, 750 (1958) [translation: Soviet Phys. JETP **35**, 521 (1959)].
[7] Amaldi, Bocciarelli, Cacciapuoti, and Trabacchi, Nuovo cimento **3**, 203 (1946).
[8] J. P. Conner, Phys. Rev. **89**, 712 (1953).
[9] J. H. Coon and R. W. Davis, Phys. Rev. **94**, 785(A) (1953); Coon, Davis, Felthauser, and Nicodemus, Phys. Rev. **111**, 250 (1958).
[10] J. R. Smith, Phys. Rev. **95**, 730 (1954).
[11] W. J. Rhein, Phys. Rev. **98**, 1300 (1955).
[12] W. G. Cross and R. G. Jarvis, Phys. Rev. **99**, 621(A) (1955).
[13] J. O. Elliot, Phys. Rev. **101**, 684 (1956).
[14] H. Nauta, Nuclear Phys. **2**, 124 (1956).
[15] L. A. Rayburn, Bull. Am. Phys. Soc. **2**, 233 (1957); *Proceedings of the International Conference on the Neutron Interactions with the Nucleus*, Atomic Energy Commission Report TID-7547 (U. S. Government Printing Office, Washington, D. C., 1957), p. 246.
[16] Berko, Whitehead, and Groseclose, Nuclear Phys. **6**, 210 (1958).
[17] Nakada, Anderson, Gardner, and Wong, Phys. Rev. **110**, 1439 (1958).
[18] Anderson, Gardner, Nakada, and Wong, Phys. Rev. **110**, 160 (1958).
[19] K. Yuasa, J. Phys. Soc. Japan **13**, 1248 (1958).